Advances in Aircraft and Spacecraft Science, *Vol. 9, No. 5 (2022) 433-447*
https://doi.org/10.12989/aas.2022.9.5.433

Lunar ascent and orbit injection via locally-flat near-optimal guidance and nonlinear reduced-attitude control

Mauro Pontani*

Department of Astronautical, Electrical, and Energy Engineering, Sapienza Università di Roma, via Salaria 851, 00138 Rome, Italy

(Received January 24, 2022, Revised May 18, 2022, Accepted May 24, 2022)

Abstract. This work deals with an explicit guidance and control architecture for autonomous lunar ascent and orbit injection, i.e., the locally-flat near-optimal guidance, accompanied by nonlinear reduced-attitude control. This is a new explicit guidance scheme, based on the local projection of the position and velocity variables, in conjunction with the real-time solution of the associated minimum-time problem. A recently-introduced quaternion-based reduced-attitude control algorithm, which enjoys quasi-global stability properties, is employed to drive the longitudinal axis of the ascent vehicle toward the desired direction. Actuation, based on thrust vectoring, is modeled as well. Extensive Monte Carlo simulations prove the effectiveness of the guidance, control, and actuation architecture proposed in this study for precise lunar orbit insertion, in the presence of nonnominal flight conditions.

Keywords: explicit guidance; lunar ascent; orbit injection; reduced-attitude control

1. Introduction

In recent years, the scientific community has shown a renewed interest toward the robotic and human exploration of the Moon, with the perspective of establishing a permanent settlement. Autonomous guidance and control in crucial operational scenarios, such as ascent, descent, and orbit docking, represents a key technological capability, especially for unmanned vehicles, such as cargo spacecraft. In particular, precision at orbit insertion represents a primary objective and affects the subsequent phases of spaceflight, because corrective maneuvers may be needed if orbit injection is completed with unsatisfactory accuracy. On the other hand, autonomous descent and landing represents a crucial task as well, and is the subject of recent research (Wang *et al*. 2022).

Traditionally, two different approaches to guidance exist. Explicit algorithms (Calise *et al*. 1998, Teofilatto and De Pasquale 1999) stem from the idea of re-defining the flight trajectory at the beginning of each guidance interval, at which an updated trajectory (leading to the target final condition) is computed. Implicit algorithms (e.g., Lu 1991) consider the perturbations from a specified nominal trajectory, and define the feedback control corrections aimed at maintaining the vehicle in the proximity of the nominal path. Neighboring optimal guidance (NOG) (Seywald and Cliff 1994, Yan *et al*. 2002, Charalambous *et al*. 1995, Hull and Nowak 1993, Pontani *et al*. 2015, Pontani and Celani 2019) can be regarded as an implicit guidance technique that relies on the

*Corresponding author, Associate Professor, E-mail: mauro.pontani@uniroma1.it

http://www.techno-press.org/?journal=aas&subpage=7 ISSN: 2287-528X (Print), 2287-5271 (Online)

analytical second-order optimality conditions, with the intent of finding the corrective control actions in the neighborhood of the reference (optimal) path. Although NOG schemes outperform all the explicit guidance algorithms, the latter have the great advantage of not requiring any nominal trajectory. Moreover, usually explicit guidance techniques are more robust than implicit algorithms. Regardless of the specific guidance scheme, the attitude control algorithm must be able to pursue the desired spacecraft orientation, usually dictated by the time-varying thrust direction yielded by the guidance. For the problem at hand, attitude control must pursue single-axis alignment, which is also known in the literature as reduced-attitude control. Significant contributions on reduced-attitude control can be found in (Chaturvedi *et al*. 2011), focused on pointing control with respect to an inertially fixed direction, and in (Pong and Miller 2015, Hu and Akella 2019), which consider reduced-attitude-tracking, corresponding to the more general case of desired time-varying pointing direction. Yang (Yang 2014) employs quaternions to design a LQR feedback controller for orbit raising. Finally, Shao *et al*. (Shao 2022) addressed the problem of attitude control in complex scenarios, i.e., in the presence of parameter uncertainties, actuator faults, and constraints on angular velocity and pointing direction.

In this study, the locally-flat near optimal guidance is presented, accompanied by a recently-introduced nonlinear quaternion-based reduced-attitude control algorithm. The latter drives the spacecraft toward the correct single-axis orientation, which is identified by assuming that the thrust is aligned with the longitudinal axis. This is in fact an approximation, because the spacecraft uses thrust vectoring, and the attitude control system must be capable of maintaining the actual spacecraft orientation sufficiently close to this thrust alignment condition. In short, the work that follows is aimed at (i) introducing a new, explicit near-optimal guidance, based on the local projection of the position and velocity variables, (ii) formulating and addressing the reduced-attitude-control problem, and (iii) modeling the actuation dynamics, based on thrust vectoring. The explicit guidance, control, and actuation methodology proposed in this study does not require preliminary offline computation of any reference trajectory or quantity. Monte Carlo simulations are run, for the purpose of ascertaining the effectiveness and accuracy of the architecture at hand, in the presence of significant displacements from the nominal initial conditions.

2. Dynamics of the ascent vehicle

This study addresses accurate lunar orbit injection of an ascent vehicle. This is assumed to be subject to the gravitational attraction of a single body (i.e., the Moon). This section describes the equations that govern both trajectory and attitude.

2.1 Trajectory

The spacecraft motion takes place about the Moon, and the dynamics of its mass center is investigated under the following assumptions:

(a) the Moon has spherical mass distribution, and

(b) the propulsive thrust is continuous and (nominally) has constant magnitude *T*.

Assumption (a) implies that the gravitational attraction is directed radially. Due to (b), the thrust acceleration a_T is

$$a_T = \frac{T}{m} = \frac{n_0}{\eta} \quad \text{where} \quad \eta := \frac{m}{m_0} \ \text{ and } \ n_0 := \frac{T}{m_0} \tag{1}$$

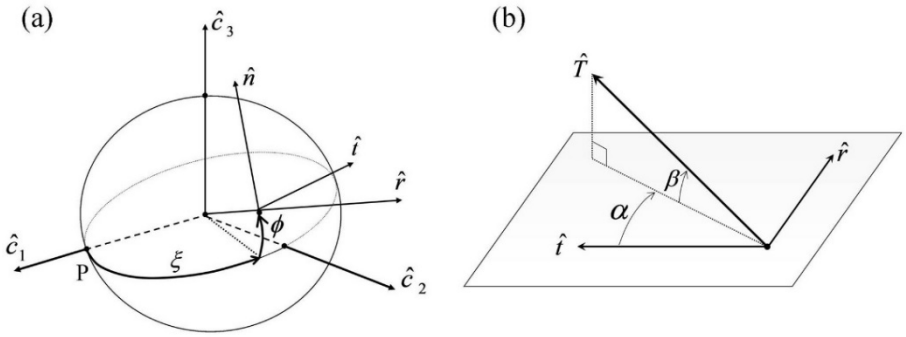

Fig. 1 Reference frames for trajectory (a) and thrust angles (b)

where m is the spacecraft instantaneous mass and m_0 denotes the respective initial value.

The ascent vehicle trajectory can be described in an inertial reference frame, associated with the right-hand sequence of unit vectors $(\hat{c}_1, \hat{c}_2, \hat{c}_3)$. Its origin is located at the center of the Moon, and the target orbit lies on the $(\hat{c}_1, \hat{c}_2)$-plane. The position can be identified by the following three variables: radius r, right ascension ξ, and declination ϕ (c.f., Fig. 1(a)). The spacecraft velocity can be projected into the rotating frame $(\hat{r}, \hat{t}, \hat{n})$, where $\hat{r}$ is aligned with the position vector $\boldsymbol{r}$ and $\hat{t}$ is parallel to the $(\hat{c}_1, \hat{c}_2)$-plane (and in the direction of the spacecraft motion, cf. Fig. 1(a)). The related components are denoted with (v_r, v_t, v_n) and termed respectively radial, transverse, and normal velocity component. The ascent vehicle is controlled through the thrust direction, defined by the in-plane angle α and the out-of-plane angle β, both illustrated in Fig. 1(b). The governing equations for $(r, \xi, \phi, v_r, v_t, v_n)$ are

$$\dot{r} = v_r \tag{2}$$

$$\dot{\xi} = \frac{v_t}{r \cos\phi} \tag{3}$$

$$\dot{\phi} = \frac{v_n}{r} \tag{4}$$

$$\dot{v}_r = -\frac{\mu}{r^2} + \frac{v_t^2 + v_n^2}{r} + a_T \sin\alpha \cos\beta \tag{5}$$

$$\dot{v}_t = \frac{v_t}{r}(v_n \tan\phi - v_r) + a_T \cos\alpha \cos\beta \tag{6}$$

$$\dot{v}_n = -\frac{v_t^2}{r}\tan\phi - \frac{v_r v_n}{r} + a_T \sin\beta \tag{7}$$

$$\dot{\eta} = -\frac{n_0}{c} \tag{8}$$

where c is the effective exhaust velocity of the propulsion system, a_T is given by Eq. (1), and μ $\left(= 4903 \frac{\text{km}^3}{\text{sec}^2}\right)$ is the lunar gravitational parameter.

2.2 Attitude

The spacecraft instantaneous orientation is associated with the body frame. Its origin is in the center of mass of the vehicle, while its axes are aligned with the right-hand sequence of unit

vectors $(\hat{\imath}, \hat{\jmath}, \hat{k})$, with $\hat{\imath}$ pointing toward the longitudinal axis. Vectrix $\underline{\underline{B}}$ is composed of $(\hat{\imath}, \hat{\jmath}, \hat{k})$, i.e., $\underline{\underline{B}} := [\hat{\imath} \quad \hat{\jmath} \quad \hat{k}]$; similarly, the right-hand sequence $(\hat{c}_1, \hat{c}_2, \hat{c}_3)$, corresponding to the inertial frame, forms vectrix $\underline{\underline{N}} := [\hat{c}_1 \quad \hat{c}_2 \quad \hat{c}_3]$.

In this research, the instantaneous attitude is referred to $\underline{\underline{N}}$ and is described through Euler parameters (quaternions), denoted with $\{q_0, \boldsymbol{q}\}$, where q_0 is the scalar part, whereas $\boldsymbol{q}$ is the (3×1)-vector part. If ${}^{N}\underline{\boldsymbol{\omega}}^{B}$ denotes the vector angular rate of $\underline{\underline{B}}$ with respect to $\underline{\underline{N}}$, the attitude kinematics equations are (Hughes 2004)

$$\dot{q}_0 = -\frac{1}{2}\boldsymbol{q}^T\boldsymbol{\omega} \tag{9}$$

$$\dot{\boldsymbol{q}} = \frac{1}{2}[q_0 I_{3\times 3} + \tilde{\boldsymbol{q}}]\boldsymbol{\omega} \tag{10}$$

where $\boldsymbol{\omega}$ denotes the (3×1)-vector that contains the three components of ${}^{N}\underline{\boldsymbol{\omega}}^{B}$ in $\underline{\underline{B}}$, i.e., ${}^{N}\underline{\boldsymbol{\omega}}^{B} = \underline{\underline{\mathrm{B}}}\boldsymbol{\omega}$, $\tilde{\boldsymbol{q}}$ is the skew-symmetric matrix associated with $\boldsymbol{q}$, and $I_{3\times 3}$ is the (3×3) identity matrix.

Under the (approximating) assumption that the mass center C does not move during the entire time of flight, the attitude dynamics equations are decoupled from the trajectory equations. Let $\mathbf{J}_C^{(B)}$ denote the spacecraft inertia matrix with respect to center of mass C, resolved in $(\hat{\imath}, \hat{\jmath}, \hat{k})$. The attitude dynamics equations are (Hughes 2004)

$$\dot{\boldsymbol{\omega}} = \left[\mathbf{J}_C^{(B)}\right]^{-1}\left(-\tilde{\boldsymbol{\omega}}\mathbf{J}_C^{(B)}\boldsymbol{\omega} - \dot{\mathbf{J}}_C^{(B)}\boldsymbol{\omega} + \boldsymbol{T}_C\right), \quad \text{with} \quad \underline{\boldsymbol{T}}_C = \underline{\underline{\mathrm{B}}}\boldsymbol{T}_C \tag{11}$$

where the (3×1)-vector $\boldsymbol{T}_C$ includes the (internal) torque components (along $(\hat{\imath}, \hat{\jmath}, \hat{k})$) due to thrust misalignment. In Eq. (11), $\dot{\mathbf{J}}_C^{(B)}$ is the time derivative of the inertia matrix, which is nonzero due to propellant consumption.

The nonlinear differential system composed of Eqs. (9)-(11) govern the instantaneous attitude and angular rate of the spacecraft. The torque components of $\boldsymbol{T}_C$ represent the control input.

The space vehicle must pursue a desired (commanded), time-varying attitude and angular rate along its ascent path. The commanded attitude is identified by vectrix $\underline{\underline{C}}$, related to the inertial frame $\underline{\underline{N}}$ through the rotation matrix $\underset{C\leftarrow N}{\mathbf{R}}$. This is associated with quaternion $\left\{q_0^{(C)}, \boldsymbol{q}^{(C)}\right\}$, whereas the commanded angular rate is ${}^{N}\underline{\boldsymbol{\omega}}^{C} = \underline{\underline{\mathrm{C}}}\boldsymbol{\omega}_C$. However, the actual body axes are associated with $\underline{\underline{B}}$, and the rotation matrix that relates $\underline{\underline{B}}$ to $\underline{\underline{C}}$ is $\underset{B\leftarrow C}{\mathbf{R}}$. This can be written in terms of the error quaternion $\left\{q_0^{(E)}, \boldsymbol{q}^{(E)}\right\}$,

$$\underset{B\leftarrow C}{\mathbf{R}} = \underset{B\leftarrow N}{\mathbf{R}}\underset{C\leftarrow N}{\mathbf{R}}^{T} = \left\{\left[q_0^{(E)}\right]^2 - \left[\boldsymbol{q}^{(E)}\right]^T\boldsymbol{q}^{(E)}\right\}I_{3\times 3} + 2\boldsymbol{q}^{(E)}\left[\boldsymbol{q}^{(E)}\right]^T - 2q_0^{(E)}\tilde{\boldsymbol{q}}^{(E)} \tag{12}$$

The kinematics equations for $\left\{q_0^{(C)}, \boldsymbol{q}^{(C)}\right\}$ are (Weiss 1993)

$$\dot{q}_0^{(E)} = -\frac{1}{2}\left[\boldsymbol{q}^{(E)}\right]^T\boldsymbol{\omega}_E \tag{13}$$

$$\dot{\boldsymbol{q}}^{(E)} = \frac{1}{2}\left[q_0^{(E)}\mathbf{I}_{3\times 3} + \tilde{\boldsymbol{q}}^{(E)}\right]\boldsymbol{\omega}_E \tag{14}$$

where $\boldsymbol{\omega}_E := \boldsymbol{\omega} - {}_{B\leftarrow C}R\,\boldsymbol{\omega}_C$. Finally, the time evolution of the rotation matrix ${}_{B\leftarrow C}\mathbf{R}$ is governed by the following equation (Weiss 1993):

$$ {}_{B\leftarrow C}\dot{\mathbf{R}} = -\tilde{\boldsymbol{\omega}}_E\,{}_{B\leftarrow C}\mathbf{R} \tag{15} $$

3. Locally-flat near-optimal guidance

This research introduces a near-optimal guidance scheme based on local projection of the spacecraft position and velocity, under the assumption that the instantaneous trajectory is sufficiently close to the $(\hat{c}_1, \hat{c}_2)$-plane, which contains the target path. This is assumed to be an elliptic orbit about the Moon, with specified periselenium and aposelenium radii, denoted with r_A and r_P, respectively. Orbit injection is assumed to occur at periselenium.

3.1 Local projection of position and velocity

The guidance algorithm is run repeatedly and starts at equally-spaced discrete times $\{t_k\}_{k=0,\dots,N-1}$. The symbol Δt_S denotes the sampling time interval, i.e., $\Delta t_S = t_{k+1} - t_k$ $(k = 1, \dots, N-2)$; the last interval is shorter, because the guidance and control algorithm stops when the desired conditions are reached with satisfactory accuracy. At time t_k, the spacecraft position and velocity are denoted with $\underset{\sim}{\boldsymbol{r}}_k$ and $\underset{\sim}{\boldsymbol{v}}_k$, and are associated with $\left(r_k, \xi_k, \phi_k, v_{r,k}, v_{t,k}, v_{n,k}\right)$ and $(\hat{r}_k, \hat{t}_k, \hat{n}_k)$ (i.e., $(\hat{r}, \hat{t}, \hat{n})$ at t_k, c.f., Fig. 1(b)). Let $(\hat{x}_k, \hat{y}_k, \hat{z}_k)$ denote three unit vectors obtained from $(\hat{r}_k, \hat{t}_k, \hat{n}_k)$ through a counterclockwise rotation about axis 2 by angle ϕ_k. Vectors $\underset{\sim}{\boldsymbol{r}}_k$ and $\underset{\sim}{\boldsymbol{v}}_k$ are projected along $(\hat{x}_k, \hat{y}_k, \hat{z}_k)$, to yield the locally flat variables $\left(x, y, z, v_x, v_y, v_z\right)$

$$ x_k = r_k \cos\phi_k \quad y_k = 0 \quad z_k = r_k \sin\phi_k \tag{16} $$

$$ v_{x,k} = v_{r,k}\cos\phi_k - v_{n,k}\sin\phi_k \quad v_{y,k} = v_{t,k} \quad v_{z,k} = v_{r,k}\sin\phi_k + v_{n,k}\cos\phi_k \tag{17} $$

These variables are governed by the following equations of motion (Pontani *et al*. 2015)

$$ \dot{x} = v_x \quad \dot{y} = v_y \quad \dot{z} = v_z \tag{18} $$

$$ \dot{v}_x = \tilde{a}_T \sin\theta_1 \cos\theta_2 - g \quad \dot{v}_y = \tilde{a}_T \cos\theta_1 \cos\theta_2 \quad \dot{v}_x = \tilde{a}_T \sin\theta_2 \tag{19} $$

where angles (θ_1, θ_2) identify the thrust direction in $(\hat{x}_k, \hat{y}_k, \hat{z}_k)$, g denotes the (local) gravitational acceleration, and $\tilde{a}_T$ is the thrust acceleration. Because the final orbit is elliptic, using $\left(x, y, z, v_x, v_y, v_z\right)$, the desired conditions at orbit injection are rewritten as

$$ x_f = r_P \quad z_f = 0 \quad v_{x,f} = 0 \quad v_{y,f} = \sqrt{\frac{2\mu}{r_P + r_A}\frac{r_A}{r_P}} \quad v_{z,f} = 0 \tag{20} $$

It is worth remarking that these projected variables are used only in the context of the guidance algorithm, and allow a sufficiently accurate approximate description of the spacecraft trajectory, provided that the time of flight is short.

3.2 Minimum-time problem

In general, the numerical solution of spacecraft trajectory optimization problems is an offline

task, which cannot be demanded to onboard guidance algorithms. In this study, the projected variables, in conjunction with the related governing Eqs. (18)-(19) and boundary conditions (20), are employed for the purpose of identifying the optimal thrust direction that minimizes the time of flight. Let $\boldsymbol{x} = [x \quad y \quad z \quad v_x \quad v_y \quad v_z]^T$ and $\boldsymbol{u} = [\theta_1 \quad \theta_2]^T$ represent respectively the state and control vector. The following optimal control problem is introduced

$$\boldsymbol{u}^*(t) = \arg\min_{\boldsymbol{u}} t_f \quad \text{subject to} \quad \text{Eqs. (18)-(20)} \tag{21}$$

where the star denotes the optimal value of the related vector.

The problem at hand admits an analytical solution that depends on the initial values of the adjoint vector conjugate to the state Eqs. (18)-(19), if $\tilde{a}_T$ and g are assumed constant in Eq. (19). To prove this, a Hamiltonian H and the auxiliary function Φ are introduced

$$H = \lambda_1 v_x + \lambda_2 v_y + \lambda_3 v_z + \lambda_4(\tilde{a}_T \cos\theta_2 \sin\theta_1 - g) + \lambda_5 \tilde{a}_T \cos\theta_2 \sin\theta_1 + \lambda_6 \tilde{a}_T \sin\theta_2 \tag{22}$$

$$\Phi = t_f + \upsilon_1\left(x_f - r_P\right) + \upsilon_2 z_f + \upsilon_3 v_{x,f} + \upsilon_4\left[v_{y,f} - \sqrt{\frac{2\mu}{r_P + r_A}\frac{r_A}{r_P}}\right] + \upsilon_5 v_{z,f} \tag{23}$$

where $\{\lambda_j\}_{j=1,\ldots,6}$ are the adjoint variables conjugate to the state Eqs. (18)-(19). The necessary conditions for optimality include the boundary conditions for the adjoint variables (Hull 2003)

$$\lambda_{1,f} = \upsilon_1 \quad \lambda_{2,f} = 0 \quad \lambda_{3,f} = \upsilon_2 \quad \lambda_{4,f} = \upsilon_3 \quad \lambda_{5,f} = \upsilon_4 \quad \lambda_{6,f} = \upsilon_5 \tag{24}$$

accompanied by the adjoint equations

$$\dot{\lambda}_1 = -\frac{\partial H}{\partial x} = 0 \quad \Rightarrow \quad \lambda_1 = \lambda_{1,0} \tag{25}$$

$$\dot{\lambda}_2 = -\frac{\partial H}{\partial y} = 0 \quad \Rightarrow \quad \lambda_2 = \lambda_{2,0} = \lambda_{2,f} = 0 \tag{26}$$

$$\dot{\lambda}_3 = -\frac{\partial H}{\partial z} = 0 \quad \Rightarrow \quad \lambda_3 = \lambda_{3,0} \tag{27}$$

$$\dot{\lambda}_4 = -\frac{\partial H}{\partial v_x} = -\lambda_1 \quad \Rightarrow \quad \lambda_4 = \lambda_{4,0} - \lambda_{1,0} t \tag{28}$$

$$\dot{\lambda}_5 = -\frac{\partial H}{\partial v_y} = -\lambda_2 \quad \Rightarrow \quad \lambda_5 = \lambda_{5,0} - \lambda_{2,0} t = \lambda_{5,0} \tag{29}$$

$$\dot{\lambda}_6 = -\frac{\partial H}{\partial v_z} = -\lambda_3 \quad \Rightarrow \quad \lambda_6 = \lambda_{6,0} - \lambda_{3,0} t \tag{30}$$

where subscript 0 denotes the value of the corresponding variable at the initial time t_0. The Pontryagin minimum principle leads to expressing the control angles in terms of the adjoint variables

$$\boldsymbol{u}^* = \arg\min_{\boldsymbol{u}} H \quad \Rightarrow \quad \begin{cases} \sin\theta_1 = -\dfrac{\lambda_4}{\sqrt{\lambda_4^2 + \lambda_5^2}} \quad \cos\theta_1 = -\dfrac{\lambda_5}{\sqrt{\lambda_4^2 + \lambda_5^2}} \\ \theta_2 = -\arcsin\dfrac{\lambda_6}{\sqrt{\lambda_4^2 + \lambda_5^2 + \lambda_6^2}} \end{cases} \tag{31}$$

The condition $\lambda_{5,0} = 0$ leads to $\theta_1 = \pm\frac{\pi}{2}$, which implies the violation of the final conditions, therefore $\lambda_{5,0} \neq 0$. Hence, the closed-form expressions of $\{\lambda_1, \lambda_3, \lambda_4, \lambda_5, \lambda_6\}$ can be scaled by $\lambda_{5,0}$, to yield

$$\sin\theta_1 = -\frac{\tilde{\lambda}_{4,0}-\tilde{\lambda}_{1,0}t}{\sqrt{\left[\tilde{\lambda}_{4,0}-\tilde{\lambda}_{1,0}t\right]^2+1}} \quad \cos\theta_1 = \frac{1}{\sqrt{\left[\tilde{\lambda}_{4,0}-\tilde{\lambda}_{1,0}t\right]^2+1}} \tag{32}$$

$$\Phi = t_f + v_1\left(x_f - r_P\right) + v_2 z_f + v_3 v_{x,f} + v_4\left[v_{y,f} - \sqrt{\frac{2\mu}{r_P+r_A}\frac{r_A}{r_P}}\right] + v_5 v_{z,f} \tag{33}$$

where $\tilde{\lambda}_{j,0} = \frac{\lambda_{j,0}}{\lambda_{5,0}}$ $(j = 1,3,4,6)$. These quantities are collected in $\boldsymbol{\lambda}_0 := \left[\tilde{\lambda}_{1,0} \quad \tilde{\lambda}_{3,0} \quad \tilde{\lambda}_{4,0} \quad \tilde{\lambda}_{6,0}\right]^T$. The analytical expressions (31)-(32) are used in Eqs. (18)-(19), and lead to obtaining closed-form solutions (not reported for the sake of conciseness) for all of the state variables

$$\begin{aligned} x = f_1(\boldsymbol{\lambda}_0, t) \quad y = f_2(\boldsymbol{\lambda}_0, t) \quad z = f_3(\boldsymbol{\lambda}_0, t) \\ v_x = f_4(\boldsymbol{\lambda}_0, t) \quad v_y = f_5(\boldsymbol{\lambda}_0, t) \quad v_z = f_6(\boldsymbol{\lambda}_0, t) \end{aligned} \tag{34}$$

Eq. (34), combined with Eq. (20), leads to a system of 5 nonlinear equations in 5 unknowns, i.e., t_f and the 4 components of $\boldsymbol{\lambda}_0$. Numerical solvers (such as the embedded routine *fsolve* in Matlab) can be employed to find the numerical solution of this system in extremely short times (of order of 0.01 sec), provided that a proper guess is supplied. To do this, the analysis described in (Pontani *et al*. 2015) can be used. In fact, for planar trajectories, corresponding to $z = 0$ and $v_z = 0$, a suitable first-attempt solution is proven to be (Pontani *et al*. 2015)

$$t_f = -\frac{v_{y,f}-v_{y,0}}{\tilde{a}_T}\frac{\tan\theta_{1,0}^{(G)}-\tan\theta_{1,f}^{(G)}}{\operatorname{asinh}\left(\tan\theta_{1,f}^{(G)}\right)-\operatorname{asinh}\left(\tan\theta_{1,0}^{(G)}\right)} \tag{35}$$

$$\tilde{\lambda}_{1,0}^{(G)} = -\frac{\tan\theta_{1,0}^{(G)}-\tan\theta_{1,f}^{(G)}}{t_f} \qquad \tilde{\lambda}_{4,0}^{(G)} = -\tan\theta_{1,0}^{(G)} \tag{36}$$

where $\theta_{1,0}^{(G)}$ and $\theta_{1,f}^{(G)}$ are two guess values for the thrust angle θ_1 at t_0 and t_f, respectively; in this work, $\theta_{1,0}^{(G)}$ is set to 80 deg, whereas $\theta_{1,f}^{(G)} = 0$. These two values correspond to a near- vertical thrust direction (at t_0) and final horizontal thrust, aligned with the desired velocity (at t_f). The remaining two guess values, for $\tilde{\lambda}_{3,0}^{(G)}$ and $\tilde{\lambda}_{6,0}^{(G)}$, are both set to 0.

The guidance algorithm repeats the preceding solution process at each sampling time t_k, which becomes the initial time t_0 of the optimal control problem. The final time t_f can be regarded as the time-to-go. However, constant values of g and $\tilde{a}_T$ are needed in each guidance interval, which has duration Δt_S. For the gravitational acceleration, the initial value is chosen, i.e., $g = \frac{\mu}{r_k^2}$. Instead, for the thrust acceleration, the average value of $\tilde{a}_T$ in $[t_k, t_{k+1}]$ is employed. Letting $n_k := \left(\frac{T}{m(t_k)}\right)$, in $[t_k, t_{k+1}]$ the thrust acceleration equals $\frac{n_k c}{[c-n_k(t-t_k)]}$. Hence, $\tilde{a}_T$ is set to

$$\tilde{a}_T = \frac{1}{\Delta t_S}\int_{t_k}^{t_{k+1}}\frac{n_k c}{c-n_k(t-t_k)}dt = -\frac{c}{\Delta t_S}ln\left(1-\frac{n_k}{c}\Delta t_S\right) \tag{37}$$

It is worth noticing that Eq. (31) resembles the linear tangent steering law (Perkins 1966, Smith 1966). However, preceding formulations of this well-consolidated guidance technique introduce approximate assumptions (Smith 1966) to solve the problem. Instead, the three-dimensional guidance approach proposed in this work is based on the real-time numerical solution of the minimum-time problem formulated in flat coordinates, through enforcement of all the necessary conditions for optimality and without any further approximation or arbitrary assumption on the

initial thrust angles θ_1 and θ_2.

3.3 Commanded attitude

The real-time numerical solution of the preceding optimal control problem provides the thrust angles (θ_1, θ_2), which identify the desired thrust direction in $(\hat{x}_k, \hat{y}_k, \hat{z}_k)$. The latter sequence is obtained from $(\hat{c}_1, \hat{c}_2, \hat{c}_3)$ through a single counterclockwise elementary rotation about axis 3 by angle ξ_k. Therefore, the commanded thrust direction $\hat{T}^{(C)}$ is

$$\hat{T}^{(C)} = [\cos\theta_2 \sin\theta_1 \quad \cos\theta_2 \cos\theta_1 \quad \sin\theta_2] R_3(\xi_k) [\hat{c}_1 \quad \hat{c}_2 \quad \hat{c}_3]^T \tag{38}$$

Under the assumption that the thrust is aligned with the longitudinal axis of the ascent vehicle, unit vector $\hat{T}^{(C)}$ identifies the commanded direction $\hat{\imath}^{(C)}$. The actual body axis $\hat{\imath}$ must be driven toward $\hat{\imath}^{(C)}$ by the attitude control system. The remaining two commanded body axes, $\hat{\jmath}^{(C)}$ and $\hat{k}^{(C)}$, are defined as

$$\hat{k}^{(C)} := \frac{\hat{c}_3 \times \hat{\imath}^{(C)}}{|\hat{c}_3 \times \hat{\imath}^{(C)}|} \quad \text{and} \quad \hat{\jmath}^{(C)} := \hat{k}^{(C)} \times \hat{\imath}^{(C)} \tag{39}$$

These three unit vectors form vectrix $\underline{\underline{C}}$, i.e., $\underline{\underline{C}} := [\hat{\imath}^{(C)} \quad \hat{\jmath}^{(C)} \quad \hat{k}^{(C)}]$. Because closed-form expressions are available for (θ_1, θ_2), the components of $\hat{\imath}^{(C)}$ (cf. Eq. (38)), $\hat{\jmath}^{(C)}$, and $\hat{k}^{(C)}$ can be written in closed form, as well as the rotation matrix that relates $\left(\hat{\imath}^{(C)}, \hat{\jmath}^{(C)}, \hat{k}^{(C)}\right)$ to $(\hat{c}_1, \hat{c}_2, \hat{c}_3)$, i.e., $\underset{C \leftarrow N}{\mathbf{R}}$. Using the kinematics equation that governs the time evolution of rotation matrices, it is straightforward to obtain the commanded angular velocity. In fact,

$$\underset{C \leftarrow N}{\dot{\mathbf{R}}} = -\tilde{\boldsymbol{\omega}}_C \underset{C \leftarrow N}{\mathbf{R}} \quad \Rightarrow \quad \tilde{\boldsymbol{\omega}}_C = -\underset{C \leftarrow N}{\dot{\mathbf{R}}} \underset{C \leftarrow N}{\mathbf{R}}^T \tag{40}$$

Because analytical expressions are available for both $\underset{C \leftarrow N}{\mathbf{R}}$ and $\underset{C \leftarrow N}{\dot{\mathbf{R}}}$, matrix $\boldsymbol{\omega}_C$ contains the closed-form expressions of the three components of the commanded angular rate ${}^N\underline{\boldsymbol{\omega}}^C$ $\left(= \underline{\underline{C}} \boldsymbol{\omega}_C\right)$ along $\left(\hat{\imath}^{(C)}, \hat{\jmath}^{(C)}, \hat{k}^{(C)}\right)$. The time derivative of $\boldsymbol{\omega}_C$ supplies $\dot{\boldsymbol{\omega}}_C$, which is necessary for nonlinear attitude control (c.f., Section 4). However, only the alignment of the longitudinal axis $\hat{\imath}$ with $\hat{\imath}^{(C)}$ is crucial for the purpose of pointing the thrust toward the correct direction. Moreover, component 1 of $\boldsymbol{\omega}_C$ is ineffective for the purpose of thrust alignment, therefore it is set to 0 (as well as component 1 of $\dot{\boldsymbol{\omega}}_C$).

4. Quaternion-based nonlinear reduced-attitude control

A recently-introduced reduced-attitude-tracking algorithm, aimed at pursuing the desired alignment for a single axis, is described and used in this research, as a suitable solution to the problem of aligning the longitudinal axis with $\hat{\imath}^{(C)}$. From inspection of the first row of $\underset{B \leftarrow C}{\mathbf{R}}$, it is apparent that correct alignment of $\hat{\imath}$ and $\hat{\imath}^{(C)}$, i.e., $\hat{\imath} \equiv \hat{\imath}^{(C)}$, corresponds to

$$\left[q_2^{(E)}\right]^2 + \left[q_3^{(E)}\right]^2 = 0 \tag{41}$$

where subscripts 2 and 3 refer to the components of $\boldsymbol{q}^{(E)}$. The latter relation is accompanied by

$$\boldsymbol{\omega}_E = 0 \tag{42}$$

Eqs. (41) and (42) identify the target set, which corresponds to the correct alignment of axis 1, whereas the commanded orientation of the remaining axes is not tracked.

4.1 Feedback law and related stability

The following two propositions provide the feedback control law for the torque components, and establish the related quasi-global stability properties. They are proven in (Napoli and Pontani 2021) and (Pontani *et al*. 2022).

Proposition 1. For the torque vector $\boldsymbol{T}_C$, the following feedback control law is introduced

$$\boldsymbol{T}_C = \tilde{\boldsymbol{\omega}}\mathbf{J}_C^{(B)}\boldsymbol{\omega} + \dot{\mathbf{J}}_C^{(B)}\boldsymbol{\omega} + \mathbf{J}_C^{(B)}\left[{}_{B\leftarrow C}\mathbf{R}\,\dot{\boldsymbol{\omega}}_C - \tilde{\boldsymbol{\omega}}_E\,{}_{B\leftarrow C}\mathbf{R}\,\boldsymbol{\omega}_C\right] - \mathbf{J}_C^{(B)}\mathbf{A}^{-1}\left[\mathbf{B}\boldsymbol{\omega}_E + \boldsymbol{f}\left(q_0^{(E)}, \boldsymbol{q}^{(E)}\right)\right] \tag{43}$$

where

$$\boldsymbol{f}\left(q_0^{(E)}, \boldsymbol{q}^{(E)}\right) := \begin{bmatrix} 0 & q_0^{(E)}q_2^{(E)} + q_1^{(E)}q_3^{(E)} & q_0^{(E)}q_3^{(E)} - q_1^{(E)}q_2^{(E)} \end{bmatrix}^T \tag{44}$$

and **A** and **B** are two constant positive definite matrices; **A** is also symmetric. The control law (43) drives the dynamical system described by Eqs. (11) and (13)-(14) toward the attracting set associated with $\boldsymbol{\omega}_E = 0$.

Because the attracting set does not coincide with the target set, Proposition 1 does not ensure asymptotic convergence toward the desired final conditions (41)-(42). However, the LaSalle's invariance principle can be used to identify the invariant set.

Proposition 2. The control law (43) drives the dynamical system described by Eqs. (11) and (13)-(14) toward the invariant set composed of the following two subsets

(1) $\boldsymbol{\omega}_E = 0$ and $\left[q_2^{(E)}\right]^2 + \left[q_3^{(E)}\right]^2 = 0$

(2) $\boldsymbol{\omega}_E = 0$ and $\left[q_1^{(E)}\right]^2 + \left[q_0^{(E)}\right]^2 = 0$

Hence, the invariant set includes two subsets, denoted with (1) and (2). It is apparent that subset (1) is the target set, whereas subset (2) corresponds to the alignment of body axis 1 toward a direction opposite to the desired one. However, convergence toward to subset (2) is only theoretical. In fact, $\left[q_1^{(E)}\right]^2 + \left[q_0^{(E)}\right]^2 = 0 \Leftrightarrow \left[q_2^{(E)}\right]^2 + \left[q_3^{(E)}\right]^2 = 1$, and this implies that V has a maximum in subset (2). Although $\dot{V} = 0$ in subset (2), if $\left[q_2^{(E)}\right]^2 + \left[q_3^{(E)}\right]^2 = 1 - \varepsilon$ (where ε is a positive and arbitrarily small constant), then $\dot{V} < 0$, and the reduction of V leads the dynamical system to converge toward the target set, i.e., subset (1) of the invariant set. In other words, subset (2) represents and unstable equilibrium, whereas the target set corresponds to a stable equilibrium. This circumstance has the very interesting practical consequence that - from the numerical point of view - the dynamical system of interest enjoys global convergence toward the desired alignment conditions, provided that the feedback control law (43) is adopted.

4.2 Gain selection

The feedback control law (43) is defined in terms of two constant, positive definite matrices,

i.e., **A** and **B**. Selection of these matrices affects the transient behavior and the convergence time of the actual attitude toward the commanded one. In this research, these two matrices are selected by assuming that both of them are diagonal and written as

$$\mathbf{A}^{-1} = c_1 \mathbf{I}_{3\times 3} \quad \text{and} \quad \mathbf{B} = c_2 \mathbf{I}_{3\times 3} \tag{45}$$

where c_1 and c_2 are two positive constants.

For the purpose of a preliminary selection of the control gains, in three-axial (full-attitude) maneuvers, the rotation is assumed to occur about the eigenaxis, and the gains of the quaternion-based nonlinear feedback law are found using the second-order equation (Weiss 1993)

$$\ddot{\varphi}_E + 2\zeta\omega_n\dot{\varphi}_E + \omega_n^2\varphi_E = 0 \quad \text{with } c_1 = 2\omega_n^2 \text{ and } c_2 = \frac{\zeta}{\omega_n} \tag{46}$$

where φ_E is the principal angle. The associated second-order system has damping coefficient ζ and natural frequency ω_n. Selection of these two parameters, which have a straightforward interpretation in relation to the transient behavior, leads to selecting two proper values of c_1 and c_2. In this study, $\zeta = 1$ and $\omega_n = 20$ sec^{-1}.

5. Actuation

The ascent vehicle employs thrust vectoring for controlling pitch/yaw attitude motion. This strategy is based on modest deviations of the direction of exhausted gases from the longitudinal axis of the spacecraft, and provides a torque action with components along body axes 2 and 3 (c.f., Fig. 2). Thrust vectoring is assumed to be implemented through deflection of the nozzle. As a preliminary step, the desired deflection angles, depicted in Fig. 2, must be obtained from the required torque $\boldsymbol{T}_C^{(C)}$, yielded by the nonlinear control algorithm. From inspection of Fig. 3(a), it is straightforward to obtain the torque due to thrust vectoring,

$$\boldsymbol{T}_C^{(C)} = \hat{\jmath} Tl \cos\Delta_z^{(C)} \sin\Delta_y^{(C)} - \hat{k} Tl \sin\Delta_z^{(C)} \tag{47}$$

This relation allows obtaining the commanded deflection angles $\Delta_y^{(C)}$ and $\Delta_z^{(C)}$, once $\boldsymbol{T}_C^{(C)}$ is known. To avoid excessive values, $\Delta_z^{(C)}$ and $\Delta_z^{(C)}$ are constrained to suitable ranges, i.e., $\left|\Delta_y^{(C)}\right| \leq 5$ deg and $\left|\Delta_z^{(C)}\right| \leq 5$ deg. The actual deflection angles Δ_y and Δ_z are driven toward the commanded values $\Delta_y^{(C)}$ and $\Delta_z^{(C)}$ by the motor, which is modeled as a first-order system (Greensite 1970)

$$\dot{\Delta}_y = \frac{\Delta_y^{(C)} - \Delta_y}{\tau} \quad \text{and} \quad \dot{\Delta}_z = \frac{\Delta_z^{(C)} - \Delta_z}{\tau} \tag{48}$$

where τ is a time constant, set to 0.1 sec.

Roll control is usually demanded to side jets. However, in this research this control action is not considered along the ascent path, and is assumed to occur, if necessary, during the subsequent phases of spaceflight.

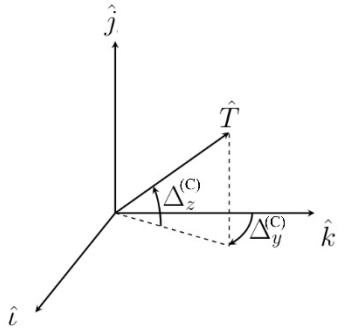

Fig. 2 Thrust deflection angles and thrust direction $\hat{T}$

6. Numerical results

The ascent vehicle has initial mass of 4700 kg (Pontani and Celani 2019), while the target elliptic orbit has aposelenium and periselenium altitudes equal to 100 km and 15 km, respectively. The propulsion parameters are $n_0 = 0.5\ \mathrm{g}_0$ ($g_0 = 9.8\ \mathrm{m/sec^2}$) and $c = 3\ \mathrm{km/sec}$. The center of mass is assumed to remain located at the same point in spite of mass depletion due to propellant consumption. Instead, the principal moments of inertia decrease, according to (Pontani and Celani 2019)

$$I_x = I_{x0} + \dot{I}_x t \quad I_y = I_{y0} + \dot{I}_y t \quad I_z = I_{z0} + \dot{I}_z t \tag{49}$$

where

$$I_{x0} = 4800\ \mathrm{kg\ m^2} \quad \dot{I}_x = -1\ \mathrm{kg}\ \frac{m^2}{sec} \tag{50}$$

$$I_{y0} = 9200\ \mathrm{kg\ m^2} \quad \dot{I}_y = -7.5\ \mathrm{kg}\ \frac{m^2}{sec} \tag{51}$$

$$I_{z0} = 8100\ \mathrm{kg\ m^2} \quad \dot{I}_z = -8.33\ \mathrm{kg}\ \frac{m^2}{sec} \tag{52}$$

The mass distribution is similar to that of the ascent module employed in the Apollo 11 mission.

A Monte Carlo (MC) campaign composed of 100 simulations is run, by assuming nonnominal flight conditions, namely (i) initial declination, with zero mean and standard deviation of 0.13 deg (corresponding to 4 km on the lunar surface), and (ii) propulsive fluctuations, modeled as stochastic oscillations about the nominal value T_{nom}, according to the following expression

$$T_{pert} = T_{nom}\left\{1 + \sum_{k=1}^{5} a_k \sin\left(\frac{2\pi t}{k t_f^*}\right)\right\}, \text{ with } a_k^{(\sigma)} = 0.04 T_{nom} \tag{53}$$

where t_f^* is the estimation of the total time of flight, obtained (offline) by solving the minimization problem described in Section 3.2 at liftoff, with nominal initial conditions. In the numerical simulations, the thrust yielded by Eq. (53) is used in Eq. (8) (setting $n_0 = T_{pert}/m_0$). Two distinct sampling intervals are adopted, i.e., 5 sec up to 250 sec after launch, and 0.5 sec for the remaining time.

Figs. 3 through 7 depict the time histories of the trajectory variables, i.e., altitude, declination, and velocity components, obtained in the MC campaign. Fig. 6 portrays the corresponding time

histories of the thrust deflection angles. Although the two angles are not clearly distinguishable, this figure points out that the limiting value (5 deg) is never exceeded. Inspection of the numerical results and the related statistics, reported in Table 1, reveals that the guidance, control, and actuation architecture at hand is very effective for precise lunar orbit injection.

Table 1 Lunar orbit injection: statistics obtained from the MC campaign

$\overline{\Delta r_f}$ (m)	$\overline{\Delta \phi_f}$ (deg)	$\overline{\Delta v_{rf}}$ (m/sec)	$\overline{\Delta v_{tf}}$ (m/sec)	$\overline{\Delta v_{nf}}$ (m/sec)	$\bar{t}_f$(sec)
1.92	7.7e−7	1.50	−0.71	9.0e−2	273.8
$r_f^{(\sigma)}$ (m)	$\phi_f^{(\sigma)}$ (deg)	$v_{rf}^{(\sigma)}$(m/sec)	$v_{tf}^{(\sigma)}$(m/sec)	$v_{nf}^{(\sigma)}$(m/sec)	$t_f^{(\sigma)}$(sec)
0.24	9.5e−6	0.64	0.73	1.00	0.33

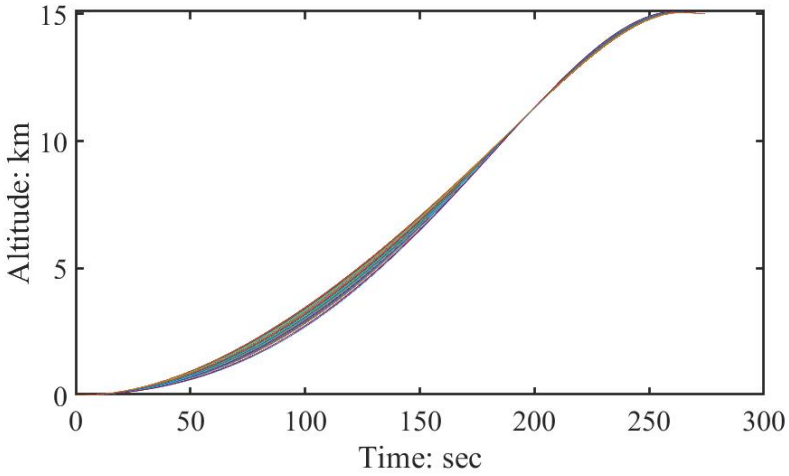

Fig. 3 Altitude time histories obtained in the MC campaign

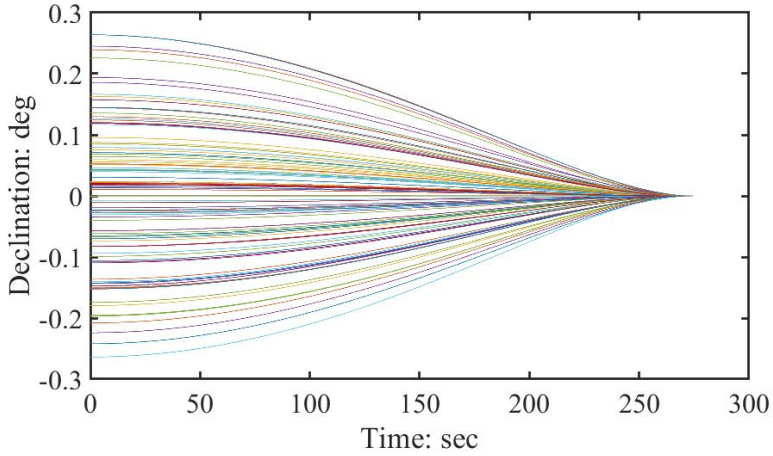

Fig. 4 Declination time histories obtained in the MC campaign

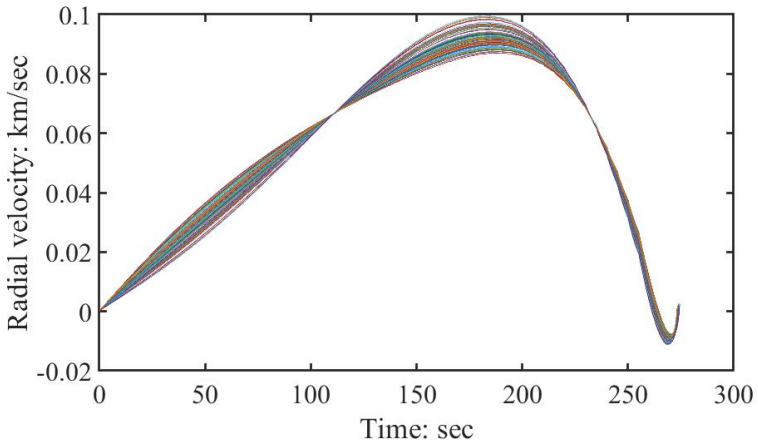

Fig. 5 Time histories of the radial velocity, obtained in the MC campaign

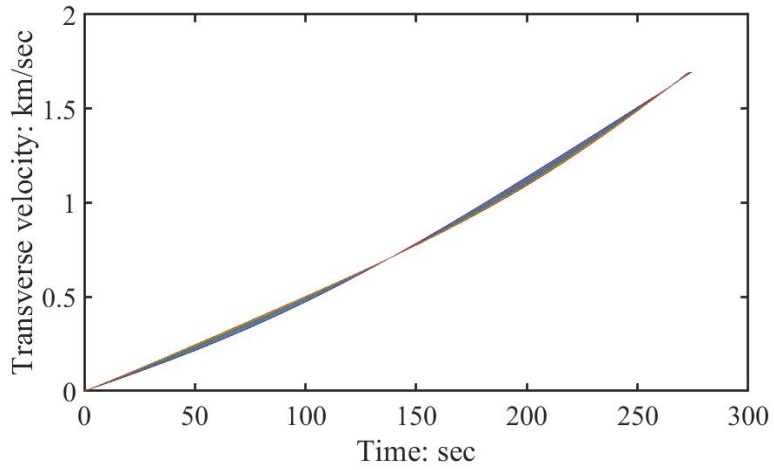

Fig. 6 Time histories of the transverse velocity, obtained in the MC campaign

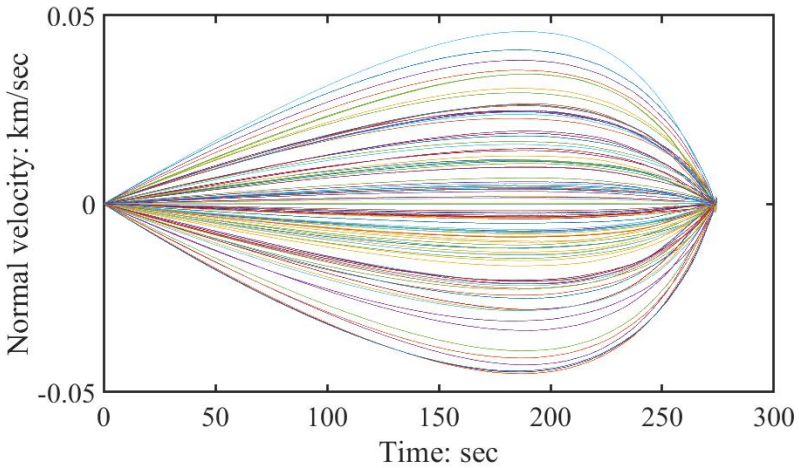

Fig. 7 Time histories of the normal velocity, obtained in the MC campaign

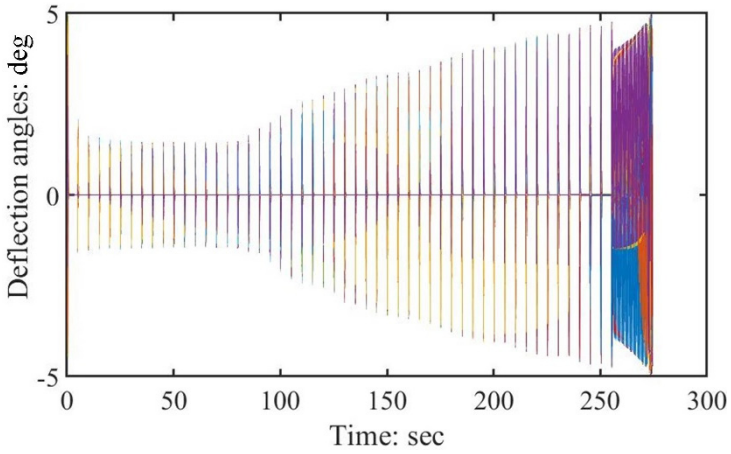

Fig. 8 Time histories of the deflection angles, obtained in the MC campaign

7. Conclusions

This study addresses the problem of autonomous lunar ascent and orbit injection using a new guidance and control architecture. An explicit near-optimal guidance is proposed as an effective strategy for the purpose of identifying the thrust direction along the ascent path. This approach is based on the local projection of position and velocity variables and the solution of an optimal control problem after its reduction to a system of 5 nonlinear equations in 5 unknowns. This is a real-time process thanks to availability of a suitable guess solution, involving intuitive variables. The two fundamental steps of the guidance algorithm, i.e., (i) local projection and (ii) numerical solution of the nonlinear equation system, are performed iteratively, at equally-spaced sampling times. The commanded thrust direction, yielded by the guidance scheme, is pursued by the attitude control system, through alignment of the actual thrust direction with the commanded one. To this end, a recently-introduced, quaternion-based nonlinear reduced-attitude control algorithm is used. Unlike three-axial control, this algorithm aims at aligning a single axis of the vehicle with a desired direction, and enjoys quasi-global stability properties. The commanded torque components represent the output yielded by the attitude scheme and the input for actuation, carried out by means of thrust vectoring. The final output of the guidance, control, and actuation architecture at hand is represented by the time histories of the two deflection angles of the nozzle. A Monte Carlo campaign is run, assuming errors on the initial conditions and significant oscillations of the propulsive thrust. The numerical results unequivocally demonstrate that the joint use of the locally-flat near-optimal guidance and the nonlinear reduced-attitude control algorithm represents an effective approach for precise lunar orbit injection.

References

Calise, A.J., Melamed, N. and Lee, S. (1998), "Design and evaluation of a three-dimensional optimal ascent guidance algorithm", *J. Guid. Control Dyn.*, **21**(6), 867-875. https://doi.org/10.2514/2.4350.

Charalambous, C.B., Naidu, S.N. and Hibey, J.L. (1995), "Neighboring optimal trajectories for aeroassisted

orbital transfer under uncertainties", *J. Guid. Control Dynam.* **18**(3), 478-485. https://doi.org/10.2514/3.21412.

Chaturvedi, N.A., Sanyal, A.K. and McClamroch, N.H. (2011), "Rigid-body attitude control", *IEEE Control Syst. Mag*., **31**(3), 30-51. httpds://doi.org/10.1109/MCS.2011.940459.

Greensite, A.L. (1970), *Analysis and Design of Space Vehicle Flight Control Systems. Control Theory: Volume II*, Spartan Books, New York.

Hu, Q., Chi, B. and Akella, M.R. (2019), "Reduced attitude control for boresight alignment with dynamic pointing constraints", *IEEE/ASME Trans. Mechatr.*, **24**(6), 2942-2952. https://doi.org/10.1109/TMECH.2019.2944431.

Hughes, P.C. (2004), *Spacecraft Attitude Dynamics*, Dover Publications, Inc., Mineola.

Hull, D.G. (2003), *Optimal Control Theory for Applications*, Springer, New York.

Hull, D.G. and Nowak, M.J. (1993), "Neighboring suboptimal control for vehicle guidance", *AAS/AIAA Space Flight Conference*, Pasadena, CA.

Lu, P. (1991), "Optimal feedback control laws using nonlinear programming", *J. Optim. Theory Appl.*, **71**(3), 599-611. https://doi.org/10.1007/BF00941406.

Napoli, I. and Pontani, M. (2021), "A new guidance and control architecture for orbit docking using feedback linearization", *Proceedings of the 72nd International Astronautical Congress*, Dubai, UAE.

Perkins, F.M (1966), "Explicit tangent-steering guidance for multi-stage boosters", *Astronaut. Acta*, **12**, 212-223.

Pong C.M. and Miller D.W. (2015), "Reduced-attitude boresight guidance and control on spacecraft for pointing, tracking, and searching", *J. Guid. Control Dyn*., **38**(6), 1027-1035. https://doi.org/10.2514/1.G000264.

Pontani, M. and Celani, F. (2019), "Neighboring optimal guidance and constrained attitude control applied to three-dimensional lunar ascent and orbit injection", *Acta Astronaut.*, **156**, 78-91. https://doi.org/10.1016/j.actaastro.2018.08.039.

Pontani, M., Cecchetti, G. and Teofilatto, P. (2015), "Variable-time-domain neighboring optimal guidance applied to space trajectories", *Acta Astronaut.*, **115**, 102-120. https://doi.org/10.1016/j.actaastro.2015.05.020.

Pontani, M., Celani, F. and Carletta, S. (2022), "Lunar descent and landing via two-phase explicit guidance and pulse-modulated reduced attitude control", *AIAA Scitech 2022*, San Diego, CA & Virtual.

Seywald, H. and Cliff, E.M. (1994), "Neighboring optimal control based feedback law for the advanced launch system", *J. Guid. Control Dyn.*, **17**(3), 1154-1162. https://doi.org/10.2514/3.21327.

Shao, X., Hu, Q., Zhu, Z.H. and Zhang, Y. (2022), "Fault-tolerant reduced-attitude control for spacecraft constrained boresight reorientation", *J. Guid. Control Dyn.*, 1-15. https://doi.org/10.2514/1.G006651.

Smith, I.E. (1966), "General formulation of the iterative guidance mode", NASA TM X-53414.

Teofilatto, P. and De Pasquale, E. (1999), "A non-linear adaptive guidance algorithm for last-stage launcher control", *Proc. Inst. Mech. Eng., Part G, J. Aerosp. Eng.*, **213**, 45-55. https://doi.org/10.1243/0954410991532837.

Wang, H., Zhang, H., Wang, Z. and Wang, Z. (2022). "Downrange estimation based on powered explicit guidance for pinpoint lunar landing", *J. Aerosp. Eng*., **35**(2), 04021129. https://doi.org/10.1061/(ASCE)AS.1943-5525.0001383.

Weiss, H. (1993), "Quaternion-based rate/attitude tracking system with application to gimbal attitude control", *J. Guid. Control Dyn.*, **16**(4), 609-616. https://doi.org/10.2514/3.21057.

Yan, H., Fahroo, F. and Ross, I.M. (2002), "Real-time computation of neighboring optimal control laws", *AIAA Guidance, Navigation and Control Conference and Exhibit*, Monterey, CA. https://doi.org/10.2514/6.2002-4657.

Yang, Y. (2014), "Attitude control in spacecraft orbit-raising using a reduced quaternion model", *Adv. Aircraft Spacecraft Sci*., **1**(4), 427-441. https://doi.org/10.12989/aas.2014.1.4.427.